AFRL-AFOSR-UK-TR-2017-0010

Flight Dynamics and Control of a Morphing UAV: Bio-inspired by Natural Fliers

Rafic Ajaj
UNIVERSITY OF SOUTHAMPTON

02/17/2017
Final Report

Air Force Research Laboratory
AF Office Of Scientific Research (AFOSR)/ IOE
Arlington, Virginia 22203
Air Force Materiel Command

REPORT DOCUMENTATION PAGE

Form Approved
OMB No. 0704-0188

1. REPORT DATE *(DD-MM-YYYY)*	2. REPORT TYPE	3. DATES COVERED *(From - To)*
17-02-2017	Final	15 Sep 2015 to 14 Sep 2016

4. TITLE AND SUBTITLE
Flight Dynamics and Control of a Morphing UAV: Bio-inspired by Natural Fliers

5a. CONTRACT NUMBER

5b. GRANT NUMBER
FA9550-15-1-0422

5c. PROGRAM ELEMENT NUMBER
61102F

6. AUTHOR(S)
Rafic Ajaj

5d. PROJECT NUMBER

5e. TASK NUMBER

5f. WORK UNIT NUMBER

7. PERFORMING ORGANIZATION NAME(S) AND ADDRESS(ES)
UNIVERSITY OF SOUTHAMPTON
UNIVERSITY RD
SOUTHAMPTON, SO17 1BJ GB

8. PERFORMING ORGANIZATION REPORT NUMBER

9. SPONSORING/MONITORING AGENCY NAME(S) AND ADDRESS(ES)
EOARD
Unit 4515
APO AE 09421-4515

10. SPONSOR/MONITOR'S ACRONYM(S)
AFRL/AFOSR IOE

11. SPONSOR/MONITOR'S REPORT NUMBER(S)
AFRL-AFOSR-UK-TR-2017-0010

12. DISTRIBUTION/AVAILABILITY STATEMENT
A DISTRIBUTION UNLIMITED: PB Public Release

13. SUPPLEMENTARY NOTES

14. ABSTRACT
An experimental investigation on using Folding wingtips sERving as cONtrol effectorS (FOLDERONS) for a mini Unmanned Aerial Vehicle (UAV was conducted). A representative off-the-shelf mini-UAV with a conventional configuration was selected. The main theme of this project is to utilize FOLDERONS as a control effectors (mainly in roll) to augment the control authority of conventional control surfaces. Furthermore, the impact of actuation rate on the effectiveness of FOLDERONS was assessed.

15. SUBJECT TERMS
EOARD, Bio-inspired, morphing, Control

16. SECURITY CLASSIFICATION OF:			17. LIMITATION OF ABSTRACT	18. NUMBER OF PAGES	19a. NAME OF RESPONSIBLE PERSON
a. REPORT	b. ABSTRACT	c. THIS PAGE			REED, SHAD
Unclassified	Unclassified	Unclassified	SAR	41	19b. TELEPHONE NUMBER *(Include area code)* 011-44-1895-616179

Flight Dynamics and Control of Morphing UAV: Bio-inspired by Natural Fliers

PI: Dr Rafic Ajaj

Grant Number: FA9550-15-1-0422

Host Organisation: University of Southampton, UK

Project Duration: 15/09/15-14/09/16

Funding Received: $15,779

Table of Content

List of Figures

This page is intentionally left blank

Summary

This report presents an experimental investigation on using FOLDing wingtips sERving as cONtrol effectorS (FOLDERONS) for a mini Unmanned Aerial Vehicle (UAV). A representative off-the-shelf mini-UAV with a conventional configuration was selected. The main theme of this project is to utilise FOLDERONS as a control effectors (mainly in roll) to augment the control authority of conventional control surfaces. Furthermore, the impact of actuation rate on the effectiveness of FOLDERONS is assessed. This report describes the preliminary and detailed design and sizing of the morphing wing. In addition, the manufacturing of the wing system and its integration with the UAV are addressed. Wind-tunnel testing in the RJ Mitchell wind-tunnel at the University of Southampton was performed. Both static (straight and sideslip) and dynamic (straight flight) testings are conducted at a range of airspeeds and angles of attack (AOAs). The impact of folding wingtips on the lateral and directional stability is analysed. The main finding of this project is that FOLDERONS are effective (especially at large dynamic pressure and AOAs) in controling the lateral and directional stability. Finally, this study shows that FOLDERONS can't fully replace conventional ailerons especially at low dynamic pressures and their strong dependence on the AOA makes them prone to a roll reversal phenomena when the wing (and FOLDERONS) is operating at negative AOAs.

I Background

From its inception, aviation has been influenced by nature. Early pioneers drew inspiration from nature, replicating patterns and mechanisms they observed. The Cody Flyer developed by Samuel Cody first flew in 1908 and is an example of how bio-inspired characteristics were used in aircraft. The wing camber could be changed by means of wire tensioners running along the wing ribs [1], much in the same way as a bird. As aviation developed, greater demand for high speed led to the development of stiffer, less adaptable aircraft structures. In the pursuit of efficiency and performance advances, the aviation industry is moving back towards bio-inspired configurations to reap the benefits of in flight adaptation and optimisation.

The commercial aviation industry is continually striving to increase the aerodynamic efficiency to meet demanding customer requirements and stringent regulations and targets such as the ACARE2020 [2]and the FlightPath2050 [3] Large wingspan is an potential solution to increase the aerodynamic efficiency, however it results in weight penalties. In addition, airports/gates sizes limits the maximum wingspan an aircraft can have. The current trend followed by Airbus and Boeing is to build airplanes with larger wingspan where the wingtips can fold up on ground to meet airport restrictions and allows larger wing span in flight maximise aerodynamic efficiency. A promising example is the Boeing 777-x which will folding wingtips allowing it to have wingspan of 71.0m compared to 64.8m for the 777-200LR. The main research question that this project aims to answer is: can these folding wingtips, that will be definitely added to be used only on the ground, be used in flight as control effectors to enhance the control authority of the aircraft? Therefore, this project is an experimental investigation to assess the effectiveness of folding wingtips as control effectors.

Previous Work

An investigation into the theoretical benefits a nd p otential f or c ontrol a ugmentation was completed by Kaygan and Gatto [4]. The base aircraft used was a commercially available flying wing which utilised a Zagi aerofoil section. The aircraft was then adapted to include a 0.15m span winglet on each tip (18% of the original span). Each winglet was assigned the degrees of freedom seen in Table 1.

Parameter	Limits	Units
Dihedral	$-90 < \Lambda < 90$	$Degrees$
Twist	$-10 < \Phi < 10$	$Degrees$
Sweep	$-40 < \Psi < 40$	$Degrees$

Table 1: Winglet Degrees of Freedom [4]

The results of interest from the study are for the dihedral deflection cases. The authors deflected the port winglet through the full range of dihedral angles whilst keeping the starboard winglet planar and the results matched previous experimental work carried out by Bourdin et al. [5]. This study numerically demonstrates the potential for roll control using folding wingtips and the conclusions are good. However, the study used a flying wing planform which is significantly different to a conventional aircraft layout, meaning the data is not directly applicable. In addition, the authors did not consider the effect of sideslip and how the yawing moments, rolling moments and stability derivatives are influenced.

Furthermore, Smith et al. [6] conducted high fidelity modelling of variable geometry wingtips using Computational Fluid Dynamics (CFD) and Vortex Lattice Method (VLM), followed by experimental validation. The study focuses heavily on lift to drag changes due to wingtip geometry with the aim of comparing the accuracies of both the prediction softwares. Testing was conducted using a single wing at a flow speed of 20 m/s. The conclusion throughout a number of comparisons is that the results are mixed but overall there is agreement in trends between both modelling techniques and the experimental data. It was highlighted by the authors that the CFD modelling technique was best suited to high speed flow and there are limitations on the accuracy of the VLM method when it comes to simulating twist and its drag sensitivity. The VLM method provides sufficient accuracy for low speed simulation.

Prior to the investigation into the theoretical benefits of morphing winglets [4], Bourdin el al. [5] and Gatto et al. [7] produced studies investigating the use of articulated winglets for flight control and load alleviation of a flying wing. The studies used the same baseline flying wing as was presented in [4] and the aim was to collect experimental data to prove the concept

of using articulated winglets for full control. A flying wing was selected so that certain winglet deflections would cause the aerodynamic centre to move in both the span-wise and chord-wise direction, allowing pitch and roll control. A system of servos was used to actuate the articulating winglets and the experimental results were good. The system showed a maximum roll authority (one winglet at 75 degree dihedral) coefficient of rolling moment change of $\Delta Cl = 0.0365$ which equates to $\Delta Cl/\Delta\Lambda = 0.0279 rad^{-1}$. By comparing this directly to the values of associated with ailerons $\Delta Cl = 0.027 - 0.087$ [7], the comparability is evident. By taking into account deflection angles, it was discussed that ailerons are more efficient per degree of deflection. This study successfully proves the validity of flying wing aircraft control using articulated winglets. The results observed are not directly applicable to conventional configuration aircraft but prove promise in this field of research. A more extensive review on folding wingtips and dihedral morphing technologies (applications and concepts) is given in Barbarino et al.[8]

It is evident from the discussion above that the study of folding wingtips is a relatively uncharted but promising field of research. Both experimental and theoretical studies have been conducted with promising results, proving the potential benefits of these systems. It is clear that there is a lack of data regarding the effectiveness of folding wingtips on a conventional aircraft configuration (fuselage, wings and tail) and no research has been carried out into the impact of these systems during a sideslip scenario. In addition, there is no knowledge of the impact of high speed actuation on folding wingtip effectiveness.

II UAV Platform

The developed winglet system has been integrated into an existing UAV platform. A conventional configuration aircraft was selected instead of a flying wing as it provides the most representative case and the results can be scaled to suit larger conventional aircraft . The selection process was based around the size constraints of the RJ Mitchell wind tunnel and ensuring the platform doesn't place unnecessary constraints on the actuation mechanism, mainly relating to the planform shape (e.g. high sweep angle). The platform selected was the Seagull Arising Star and can be seen in Figure 1. The chosen platform is a highly regarded trainer aircraft with a rectangular wing planform. The low aspect ratio wing means that the tip vortex is strong and it will receive large benefits from the addition of winglets [9] .

Figure 1: Seagull Arising Star V2 UAV platform
[10]

The Arising Star uses a flat bottom aerofoil profile with a cambered upper surface, making it very stable. For simplicity, the prototype design utilises a NACA0018 symmetric aerofoil to maximise the volume within the wing and reduce the size limitations placed upon actuation design. Flight characteristics of the modified aircraft are identical to those of the donor aircraft and can be seen in the following table:

Parameter	**Value**	**Units**
Wing Span	1.6	m
Wing Area	0.416	m^2
Average Chord	0.26	m
Maximum Flight Speed	20	m/s

Table 2: Arising Star wing specification

III FOLDERONS

A conceptual design phase was carried out and the concepts developed offer a wide range of solutions to the proposed problem, each with their own merits. A down-selection process was then carried out to develop the final concept.

A Actuation Concepts

Concept 1

Concept 1, shown in Figure 2, investigates the use of hinge line actuators to develop the rotational torque required. The advantage of this design is that the direct connection between the actuators and the hinge line mitigates additional transmission losses making the system more efficient. The biggest disadvantage is the loss in winglet area due to the mounting position of the actuator. The majority of the recovered vortex energy is located near the trailing edge of the wing, so provided this loss in area is kept relatively small, this is acceptable. A further disadvantage by locating the actuator in this position is that it is susceptible to damage should the aircraft have a tip strike upon landing or take off. In addition, the actuator mass will maximise the root bending moment in this position.

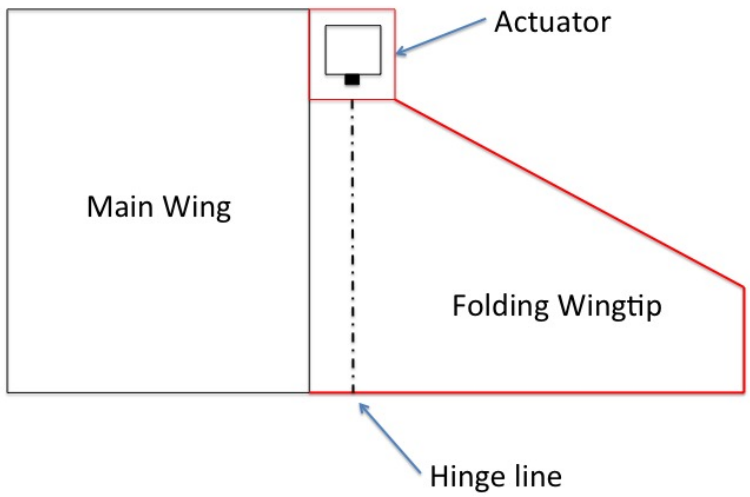

Figure 2: Concept 1 utilising hinge line actuators (Top View)

Concept 2

Concept 2, shown in Figure 3, aims to maximise the winglet surface area and bring the actuation components inboard. A system of timing pulleys and belts has been used to transfer the actuation torque to the hing line. In comparison to concept 1, higher transmission losses will be observed and this is to be controlled through the use of bearings. There are bearings placed

next to the actuator to ensure there is no lateral load placed upon the actuator itself. Regular maintenance to check belt tensioning and to service the bearings is a major disadvantage to this design.

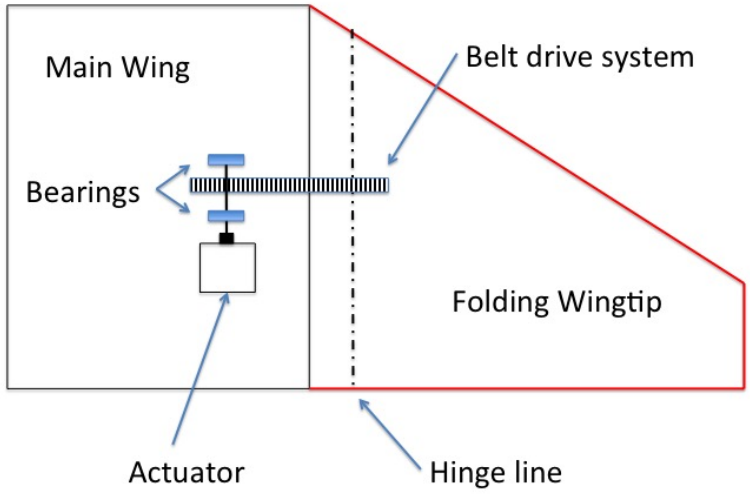

Figure 3: Concept 2 using a system of pulley gears (Top View)

Concept 3

Concept 3, shown in Figure 4, uses a worm drive to transfer the torque. The major advantage to this system is the power off locking capability. If the lead angle on the screw is selected carefully, the wheel cannot rotate unless the screw is actively driven. This means zero power is required for the system when remaining in 1 state. These benefits for the current application might however be limited as the system will be continually changing state. The worm drive acts to gear the system, enabling larger torques to be developed. This could be advantageous by allowing a less powerful (smaller) actuator to be used but it will also make the system slower. The report focuses on high speed actuation so this is a major issue. The mounting arrangement of worm gears means that the actuator must sit below or above the centreline, this reduces the already limited size available to fit an actuator.

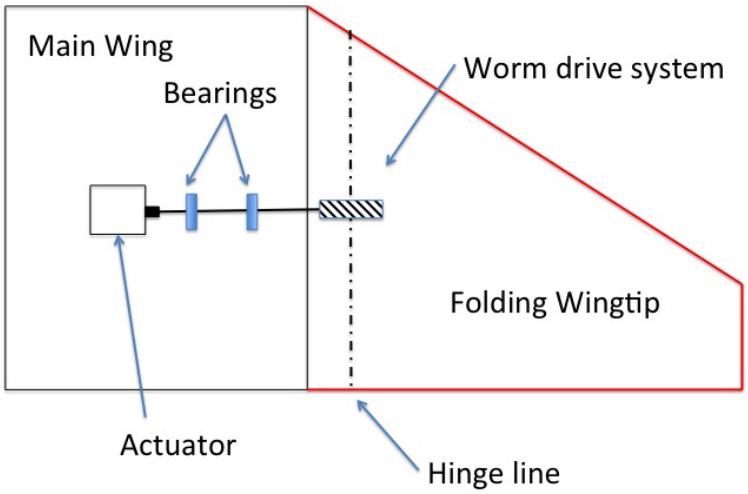

Figure 4: Concept 3 using a worm gear system (Top View)

Downselect

To select the optimal solution, the design concepts were rated against the following criteria; cost, complexity, estimated mass, robustness and effectiveness. The optimal solution to meet these requirements is concept 2, the belt drive solution.

B Gap Covering Concepts

The space between the tip of the main wing and the root of the winglet is a critical region. With any form of actuation there will be a gap between these parts allowing air to escape through and reduce the efficiency. The level to which this gap has an impact is yet to be quantified but consideration has been given to the problem. Two major ideas have been investigated to solve this problem. The first is to completely cover the region using some form of skin. The second is to reduce the gap to as little as possible.

Fully Covered Method

Previous studies have shown that corrugations are an effective method to bridge the gap but are aerodynamically poor according to Ursache et al [11] and should be avoided. Flexible skin such as latex is an idea investigated by the authors with a moderate amount of success, as shown in

Figure 5. This is aerodynamically superior to corrugations but the amount of tension required to keep a smooth surface during high dihedral folding is excessive. This method places significant extra loading on the actuation components, leading to larger actuators which reduces any potential aerodynamic efficiency benefit. Another concept investigated is the use of a retractable skin, this mitigates the issues relating to the flexible skin tensioning but introduces significant complexity. The conclusion is that until the impact of not covering the area is quantified and shown to be significant, there is not a viable solution when considering mass and complexity.

Figure 5: Flexible latex skin investigation

Gap Reduction Method

The alternative method is to not directly solve the problem but to reduce the impact of it. This method aims to reduce the gap between the wingtip and the winglet to minimise the leakage between the upper and lower surfaces. The challenging part to this project was that the wingtip is designed to move 180 degrees and a gap reduction method must account for this. The concept generated acts in a similar way to classical aileron hinges, utilising a semicircular leading edge. Due to the high degree of dihedral proposed for the system, a wingtip section encapsulating the semicircular profile is not possible in the same way as it is on ailerons. The concept uses a ver-tical face on the inboard section to allow the full 180 degree motion required. The semicircular section on the wingtip ensures a minimal gap is maintained through all angular displacements.

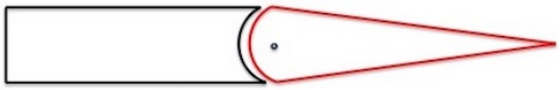

(a) Aileron style hinge with encapsulating inboard section preventing full range of motion (Front View)

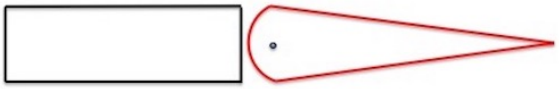

(b) Selected hinge style to enable full range of motion (Front View)

Figure 6: Gap reduction hinge designs

IV Modelling and Sizing

Tornado Vortex Lattice Method (VLM) was used for aerodynamic prediction. Tornado is a Vortex Lattice Method software programmed in MATLAB; it was selected due to its fast solving time and ability to be controlled through custom MATLAB scripts. Tornado VLM models the wing as thin sheet of discrete vortices and computes the pressure and force distributions around the whole body. The aerodynamic coefficients are then derived directly from these. The analysis has been run at the ultimate operating condition for the aircraft, which corresponds 15 degrees AOA and 20 m/s airspeed, to estimate the maximum loads on the wing. After inputting the geometry and the test conditions through a binary based user interface, the simulation can be run in very little time. The aerodynamic loads extracted from Tornado are used to size the wing/wingtip structure and to size the actuation system. At 20m/s and 15 degrees AOA, the main wing lift is 117.4N and the wingtip lift is 6N.

Structural Layout

The wind-tunnel prototype has 2 mounting ribs located on the main wing to allow attachment and load transfer to the overhead load cell. The aerodynamic loads generated by the main lifting surface are transferred to these ribs via 2 main wing spars running the full span of the wing, as shown in Figure 7a. Mounted directly onto the ends of the spars are the folding wingtips and associated actuation components for efficient load transfer. The fuselage complete with tail surfaces and landing gear is mounted underneath the wing using 8 diagonally placed rubber bands. This attachment method is identical to the original aircraft and one that was shown to be structurally robust.

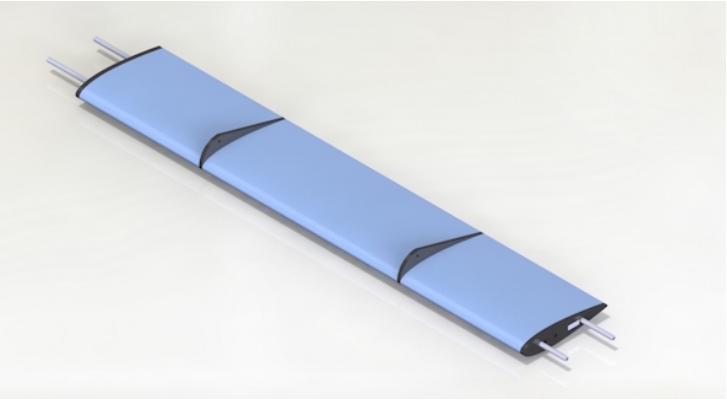

(a) Wing structure including main spars and ribs

(b) Main wing cross-section showing internal cutouts for main spars and electrical cable runs

Figure 7: Main wing structural layout

Spar Sizing

The 2 main spars give the wing structural rigidity and allow the aerodynamic loads to be transferred from the extruded polystyrene wing profiles to the overhead load cell. The spars have been sized using classical bending theory and a number of assumptions to analyse commercially available tubing:

Modelling assumptions:

- The wing is treated as a half span canterleaver beam
- The 2 spars share the load equally
- A safety factor of 1.25 is used due to the unmanned nature of the aircraft [12]

Actuation Components

The torque required was calculated by summing the elementary factors of moments around the wingtip hinge line whilst operating at 20m/s and 15 degrees AOA (worst case scenario). All forces were assumed to act at the midspan of the wingtip creating a conservative requirement. In addition, a 20% safety factor was included in the final value to account for any uncertainties and prevent transmission slip [13]. The final torque requirement was 1.459 Nm

From the finalised torque requirement, an actuator and transmission system were sized. The servo motor selected was the DFROBOT 180 degree standard servo that can supply 1.47Nm of

torque when supplied with 7.2V. The pulleys and timing belt combination have been sized for a 1:1 ratio and this has been completed as follows.

The value of specific torque taken from a relevant manufacturer data sheet is 1.7 and through analysing the systems available, the final system was designed. It was found that a 1cm wide belt coupled with two 14 tooth T5 timing pulleys provided the smallest system capable of meeting the requirement. The transmission system specified is able to transfer 1.67 Nm of torque, 15% higher than the maximum servo torque.

V Wind Tunnel Demonstrator

The prototype has been designed with modularity being a key philosophy. Units can be removed for modification or maintenance purposes. The main wing is constructed from 2 spars running through extruded polystyrene foam and secured onto the tips of the main wing are the FOLDERONS which houses all the actuation components and the wingtip itself. Two wind tunnel mounting ribs are secured directly to the spars and act to transfer load to the overhead wind tunnel balance.

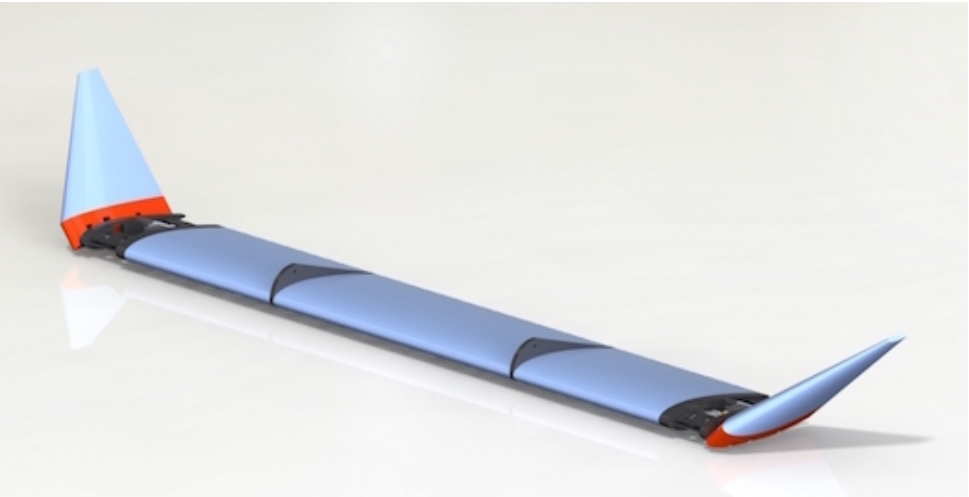

Figure 8: Full prototype design

A FOLDERONS Structure

The structural component of the FOLDERONS are manufactured from laser cut 6mm birch plywood. Laser cutting was chosen due to its low cost and high accuracy, an accuracy of $\pm 0.2mm$ is achievable depending upon material. This method combined with Computer Aided Design (CAD) allows complex wood joints to be created with relative ease. Finger joints were integrated into the supporting braces to connect them securely to the main ribs. The finger joints significantly increase the surface area available for glueing and this, combined with the interlocking element between components, makes them very strong. The resultant part can be seen in Figure 9:

(a) Inboard side of FOLDERONS structure

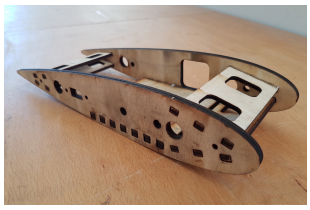

(b) Internal joint structure

(c) Outboard side of FOLDERONS structure

Figure 9: FOLDERONS structure manufactured from 6mm birch plywood

The next stage in the FOLDERONS manufacture was to install the actuation components. The bearing rod ends were installed into the pre cut mounting holes using nuts and washers. Following the bearing installation, a custom rotating bar was manufactured using a lathe. The bar was manufactured from 8mm mild steel and sized to fit between the two outboard bearings with a 5mm thread cut into both ends to secure it in place. The timing pulleys and belt were then installed and secured using a grub screw. The servo motors were installed into the FOLDERONS using a Computer Numeric Control (CNC) machined aluminium mount secured in place using 4 mounting bolts. Four mounting points provide a secure base for the actuator and prevent any movement resulting from torque reactions. The actuator was connected directly to the inner pulley drive shaft via a quarter inch brass shaft connector and 4mm grub screw. The installation can be seen in Figure 10.

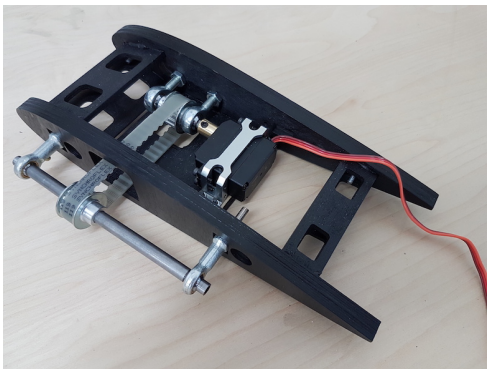

(a) Final actuator installation

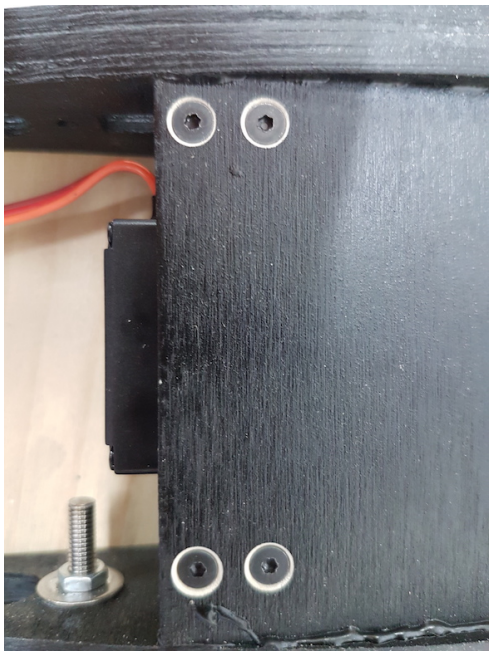

(b) Countersunk actuator mounting bolts

Figure 10: Final installation of the servo motor actuator

To secure the FOLDERONS to the main wing, two 6 mm neodymium magnets were installed. A custom made 3 pin connector was developed and installed to allow the FOLDERONS electrical connection to be easily connected and disconnected.

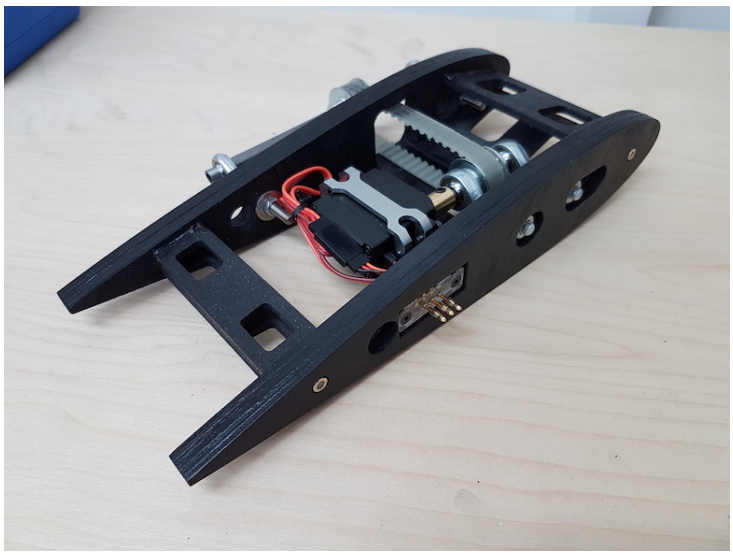

Figure 11: Assembled modular tip unit

The wingtip was cut using CNC hot wire cutting and the process created a burn away channel in the surface. To rectify this, a polyester filler was used to create a smooth aerodynamic finish. The gap reduction module was 3D printed out of ABS plastic to allow complex internal geometry. Before the wingtip spars were installed, shaft couplers were welded on to enable the entire wingtip section to be removed for modification or maintenance. The spars were then bonded into the gap reduction module and wingtip section to form the final component. Plastic covers were secured onto the units to cover the actuation components

Main Wing

The main wing is manufactured from extruded styrofoam and the process was completed by CNC hot wire cutting due to it's high precision. The material was selected due to its low cost and compatibility with hot wire cutting. Each section has an internal cut out for both spars and an internal wiring channel for electrical connections. These sections were glued onto the spars along with the wind tunnel mounting ribs to form the final wing. The channel left by the wire cutting process has been smoothed using a polyester filler.

Figure 12: Assembled Wing

An Arduino was used to control the actuators and a series of codes were developed to allow specific tests to be carried out. Once the final assembly was finished, bench testing was completed to tune the control codes and correctly tension the belt drive transmission.

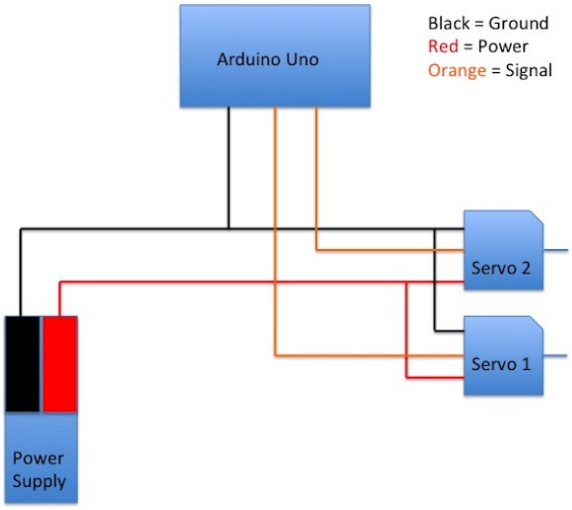

(a) A schematic to show the electrical connections of 2 servo motors and an arduino

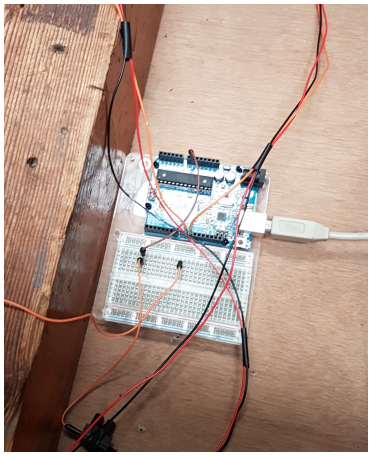

(b) The Arduino layout during tunnel testing

Figure 13: Arduino controller used during testing

VI Wind Tunnel Testing

The RJ Mitchell wind tunnel at the University of Southampton was used for testing the prototype. A 6-axis overhead load cell with a data acquisition rate of 1 kHz is mounted on a overhead turntable, allowing sideslip scenarios. Using a turntable means that during sideslip testing, the forces are along the axes of the aircraft and not the axes of the wind tunnel. The prototype was mounted using two main vertical struts attached to the mounting ribs of the main wing and a tail strut attached to the rear of the fuselage, as shown in Figure 14. The tail strut enabled the AOA to be changed from within the control room. The testing was completed without an engine or propeller being installed and the resulting data neglects these features. Prior to any testing occurring, the load cell was calibrated and tare values at all conditions were recorded. Three types of testing were conducted to analyse the effectiveness of FOLDERONS; Static forces, Dynamic data and Sideslip data. During each test, the following data was recorded; Lift(N), Drag(N), Sideforce(N), Rolling Moment(Nm), Yawing Moment(Nm) and Pitching Moment(Nm)

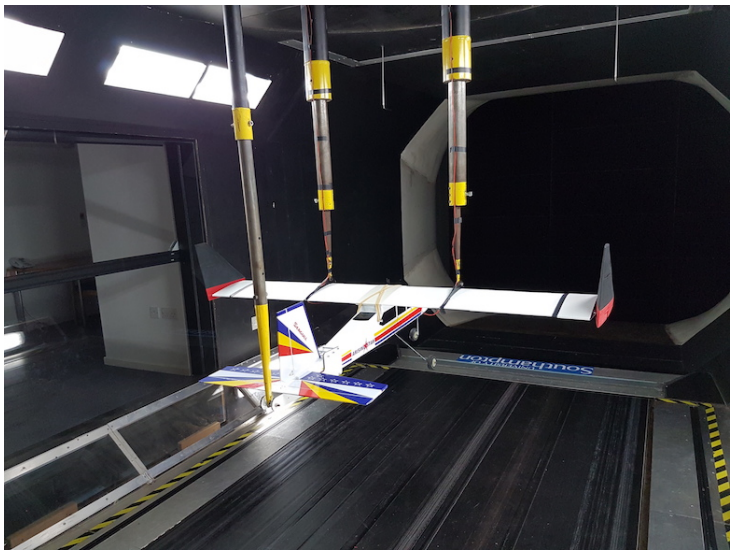

Figure 14: UAV Installation in the RJ Mitchell Tunnel

Static Testing - No Sideslip

The first test series was static forces in a series of wingtip configurations, airspeeds and AOA's. A wide range of flight conditions were selected to show data trends through various flight phases such as take off, climb and cruise. The testing parameters are shown in Table 3 below:

Parameter	Test Values	Units
Left Wingtip Dihedral	-90, -60, -30, 0, 30, 60, 90	$Degrees$
Right Wingtip Dihedral	-90, -60, -30, 0, 30, 60, 90	$Degrees$
Airspeed	10, 15, 20	m/s
AOA	0, 5, 10, 15	$Degrees$

Table 3: Static Testing Parameters

The static testing process was an iterative one. Firstly, the angle of attack and airspeed were set to a desired value. Once the airspeed had settled, the wingtip actuation code was uploaded to iterate through all possible wingtip configurations, as specified in Table 3. The code was set to pause at each configuration for a 15 second interval, during which data was recorded. A 5 second data set was recorded at 1 kHz (5,000 data points) and then averaged automatically before being appended into a text file. An example of the test configurations can be seen in

Figure 15.

(a) Symmetric deflection

(b) Asymmetric deflection

Figure 15: An example of static deflection cases

Dynamic Testing

The second testing series was to investigate the aerodynamic impact of high speed actuation. In order to test this, the same airspeed and AOA values as presented in Table 3 were used to allow comparisons between static and dynamic to be made. The wingtip configurations however, took a different form. One wingtip was set to move to a position and hold whilst the other wingtip completed a full speed sweep from -90 to +90 degrees, during which data was collected. The aim of this test series is to gain insight into the transient behaviour, so for each test case the raw data was captured without an automated averaging process. A four second data window was captured to allow sufficient time before and after the event to make post processing more effective. The speed of actuation was kept constant to reduce the number of variables and a full 180 degree sweep was recorded to take 0.79s at zero degrees angle of attack.

Static Testing - Sideslip

The sideslip testing procedure was almost identical to that of static testing, the only difference being the addition of the sideslip angle variable. A range of test variables were used to gather data over various flight phases and details of these can be seen in Table 4:

Parameter	Test Values	Units
Left Wingtip	-90, -60, -30, 0, 30, 60, 90	$Degrees$
Right Wingtip	-90, -60, -30, 0, 30, 60, 90	$Degrees$
Airspeed	10	m/s
AOA	0, 5, 10, 15	$Degrees$
Sideslip	5, 10	$Degrees$

Table 4: Sideslip Testing Parameters

VII Results and Discussion

A Static Forces as a Result of Wingtip Folding

Rolling Moment Variation

The data presented in Figures 16 - 19 is the rolling moment coefficient variation for all four angle of attack cases at 15 m/s airspeed. The data trends for all 3 airspeeds are near identical with only their magnitudes varying. For this reason, only one data set has been repeated here. Each data series within a plot represents the rolling moment coefficient variation with a constant port dihedral and varying starboard dihedral angle. The legend to the south describes the port dihedral state.

By observing Figures 17, 18 and 19 it is evident that for each port winglet data series, the minimum point lies at negative 30 degrees starboard dihedral. This minimum point represents the position where the starboard wingtip is producing maximum lift and the rolling moment coefficient is at its greatest and in an anti-clockwise direction. This observation is valid for almost all cases where the AOA > 0. In all the zero degree AOA cases (over all three airspeeds) instead of the minimum lying at negative 30 degrees dihedral, there is a maximum observed at positive 30 degrees dihedral. This can be seen in Figure 16. The switch from a minimum to a maximum shows that the aircraft is producing a rolling moment in the opposite direction to the higher angle of attack cases. From this, we can conclude that the aircraft is producing downforce and thus explain the shift from a minima to a maxima. This also explains why the aircraft is now producing its maximum rolling moment at positive 30 degrees.

By taking the case of zero degrees port dihedral and ninety degrees starboard dihedral at

a positive angle of attack, the aircraft will produce a clockwise rolling moment. At negative angle of attack, this same configuration produces an anti-clockwise rolling moment. From a pilot's (or autopilot's) perspective, this has the potential to cause a dangerous situation. This must therefore be considered in an aircrafts flight control system.

The main conclusion that can be drawn from this testing case is that $\pm$ max(Lift) is almost always achieved at a wingtip dihedral angle of ± 30 degrees, not at zero degrees as might be expected. It should be noted that due to the dihedral increments of 30 degrees used in this study, the true maximum lift value might lie somewhere between 0 and 30 degrees but we can conclude it does not lie at zero degrees.

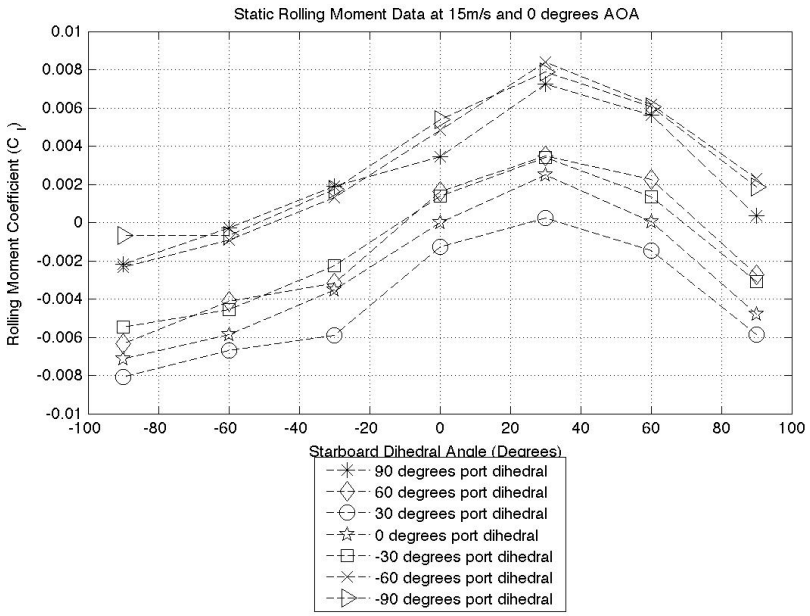

Figure 16: 0 degrees AOA static test results

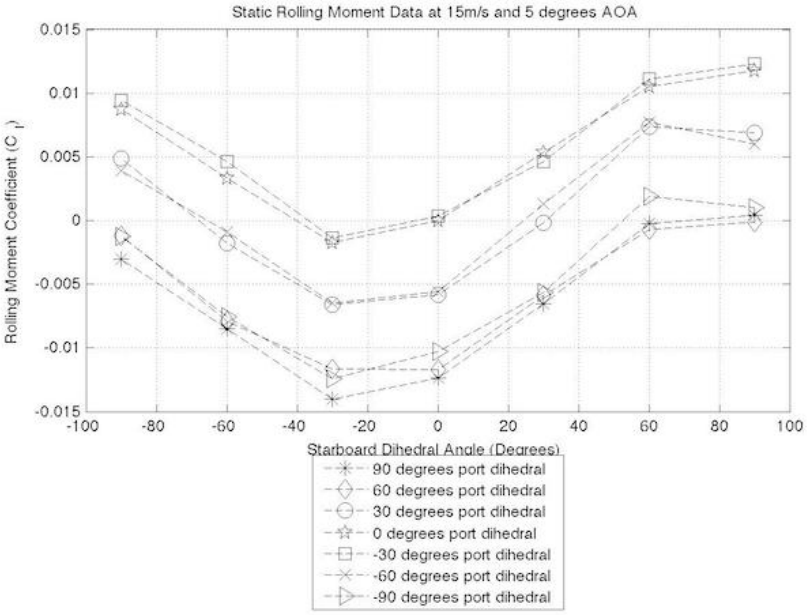

Figure 17: 5 degrees AOA static test results

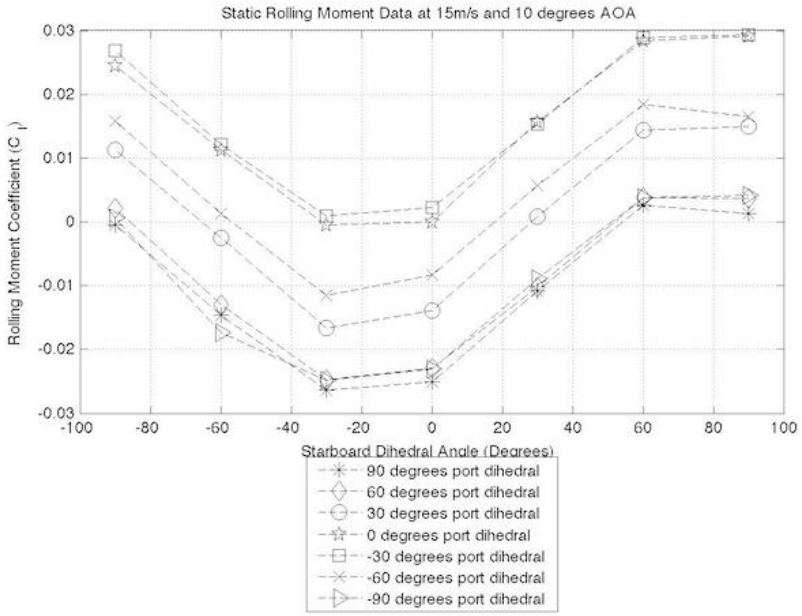

Figure 18: 10 degrees AOA static test results

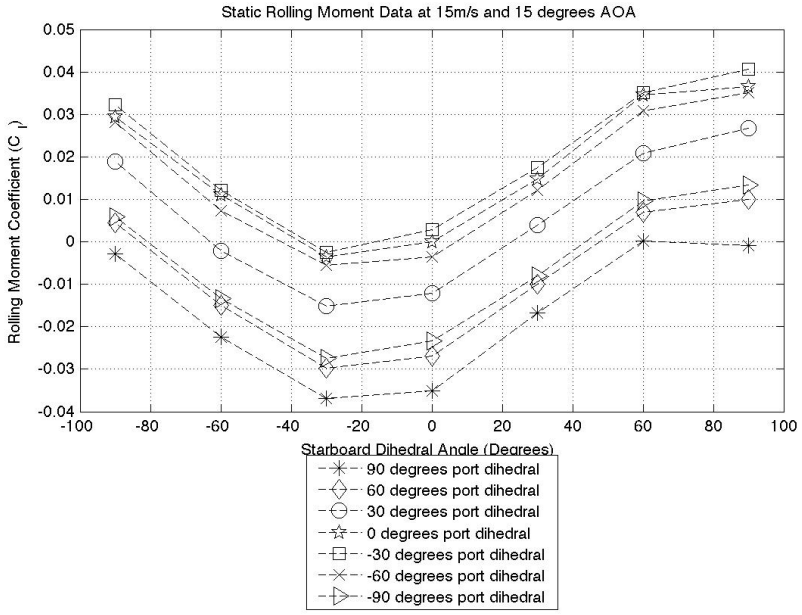

Figure 19: 15 degrees AOA static test results

Aileron Comparison

Table 5 below shows the maximum port (negative) and starboard (positive) rolling moment (Nm) recorded at each airspeed and AOA. By observing the table, it can be seen that the magnitude increases with airspeed and AOA, as expected.

Table 5: Maximum and minimum rolling moments at different flight conditions

	AOA (Degrees)			
Airspeed (m/s)	*0*	*5*	*10*	*15*
10	-0.4 : 0.42	-0.79 : 0.65	-1.47 : 1.32	-1.16 :2.95
15	-1.04 : 0.78	-1.75 : 1.15	-2.81 : 3.33	-4.06 : 4.48
20	-2 : 0.82	-3.04 : 2.75	-5.7 : 5.7	-6.5 : 7.6

The maximum and minimum rolling moment coefficient range is $\Delta Cl = 0.008 - 0.039$ and when compared to ailerons $\Delta Cl = 0.027 - 0.087$ [7] the results are in the same order of magnitude. At low AOA and airspeed (0 degrees and 10 m/s, respectively), the ΔCl value is significantly lower than that of ailerons. As the AOA and airspeed increases (maximum at 15 degrees and 20 m/s, respectively), the ΔCl value moves to within the central limit of the

aileron values. This is an excellent result and is inline with the result shown in [7] but with a slightly higher value of maximum rolling moment coefficient. When the deflection angle is taken into account, ailerons however prove to be more effective at generating a higher rolling moment with a lower deflection angle, once again inline with the results shown in [7].

The poor performance observed at low AOA and low dynamic pressure can be explained using an approximate rolling moment (Equation 1). The derived equation assumes that the wingtips' AOAs is the same as the main wing. Equation 1 shows that the rolling moment is directly proportional to AOA and dynamic pressure To alleviate this problem, the AOA of the wingtip could be changed at certain flight conditions but this would add significant complexity and will cause the aircraft to be prone to tip stall.

$$L=1/2\rho V^2 S_w C_{L\alpha}\alpha(b/2)[\cos(\Lambda_2)-\cos(\Lambda_1)] \quad (1)$$

The variables in Equation (1) are defined in the nomenclature section. The conclusion can therefore be made that on a conventional aircraft, FOLDERONS cannot be used to fully substitute conventional ailerons at low speed flight phases but have the potential to augment the rolling authority delivered by conventional ailerons. It should be noted that the rolling moment generated by FOLDERONS is nonlinear relative to the dihedral angle of the wingtips making its integration with the linear flight control system more difficult.

B Effect of High-Speed Actuation on System Performance

To reduce the data noise generated through high frequency data collection, the data has been averaged in blocks of 40 to reduce the 4,000 data points recorded down to 100 averaged points. A moving average has also been fitted through this data for visualisation purposes. A further piece of code has been written to overlay the static data onto the dynamic data and produce data plots for direct comparisons.

A sample of this data can be seen in Figure 20 and represents the trend seen throughout.

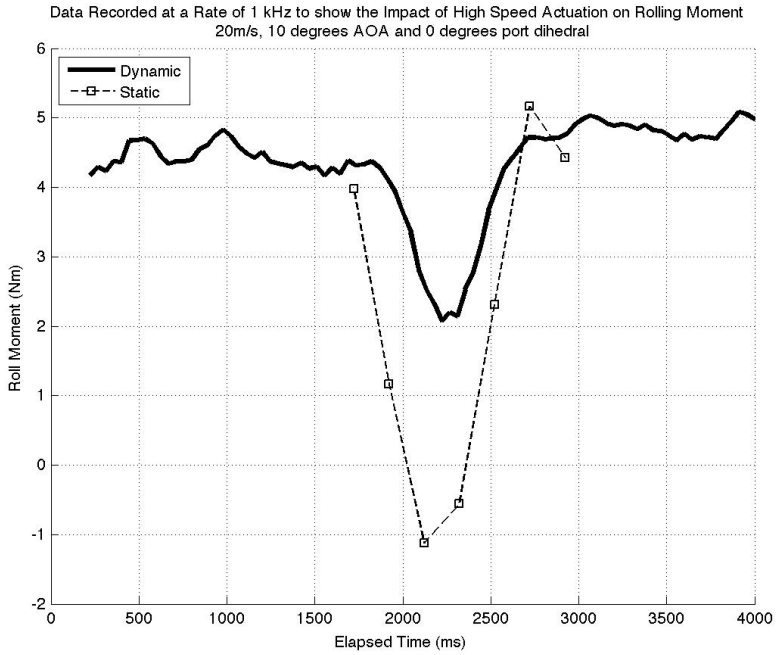

Figure 20: Dynamic vs Static results

The data clearly shows a discrepancy in the rolling moment produced by the static and dynamic cases. In this data series, the static data represents the maximum rolling moment available at that configuration as there is no negative effects as a result of actuation impacting this value. The high speed actuation during the dynamic data collection clearly results in a reduction in rolling moment in all configurations. From this we can conclude that the wingtip surface is moving faster than the airflow settling time and the rolling moment is not meeting its full potential. This is a significant result and shows that high speed actuation has a detrimental impact upon the effectiveness of FOLDERONS.

C The Effect of Folding Wingtips on Aircraft Stability During a Sideslip Scenario

The sideslip analysis consists of two parts, the directional stability and the lateral stability. The changes in stability values as a direct result of wingtip folding is the critical aim, not the stability values themselves.

Lateral Stability

Figures 21 and 22 show a comparison of the lateral stability for 5 degrees and 10 degrees sideslip respectively. Both cases are at 10 m/s airspeed and 10 degrees AOA and both are a representation of the trends seen in all data cases.

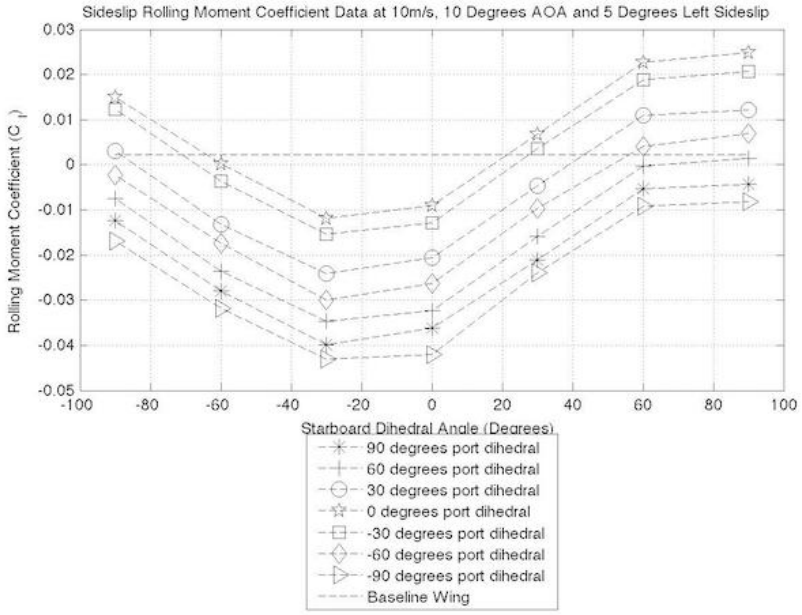

Figure 21: 5 degrees sideslip rolling moment coefficient

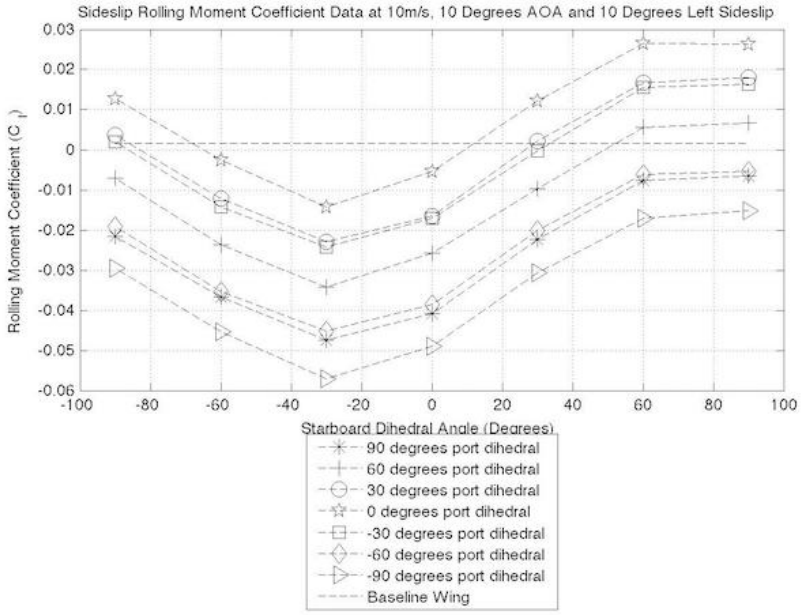

Figure 22: 10 degrees sideslip rolling moment coefficient

By observing the baseline wing data line, it can be seen that the aircraft is only slightly laterally stable, and the removal of dihedral is likely to have caused this. Both Figures 21 and 22 clearly show that at certain configurations, the wingtips can produce a restoring moment and create a stable aircraft. They also show how the wingtips can induce an instability. By observing the data, the configuration producing maximum restoring moment is a low port dihedral (0 / $\pm$30) and a high positive starboard dihedral angle (60 / 90), the combination of which is dependent upon flight condition. This broadly agrees with the results found in the static data analysis regarding rolling moment at zero degrees sideslip.

By symmetrically deflecting the FOLDERONS upward, the aircraft is temporarily increasing its level of dihedral at the outer portions of the wing. The data generated shows that through symmetric deflection, the dihedral effect can be observed. By symmetrically deflecting to positive angles, the restoring moment is increased over the planar case and at high sideslip angles, it exceeds the baseline wing. The impact of anhedral is also observed and symmetric deflection downwards reduces the lateral stability in comparison to a planar wing, for example a negative 60 degree symmetric deflection. This is a significant result and shows that FOLDERONS have the ability to be used for temporary dihedral/anhedral increases.

It has been shown that the lateral stability can be increased by two methods; asymmetric deflection to create a lift differential or symmetric deflection to induce the dihedral effect. From the data plots presented, the most effective method is through asymmetric deflection.

Real Aircraft Lateral Stability Comparison

To quantitatively analyse the effectiveness of FOLDERONS upon lateral stability, the lateral stability derivative, $C_{l\beta}$, has been plotted and the resulting graph can be seen in Figure 23. For a left hand sideslip, the lateral stability derivative should be negative for a stable aircraft. A negative value means that the restoring moment rolling the aircraft away from the sideslip increases with an increase in sideslip angle.

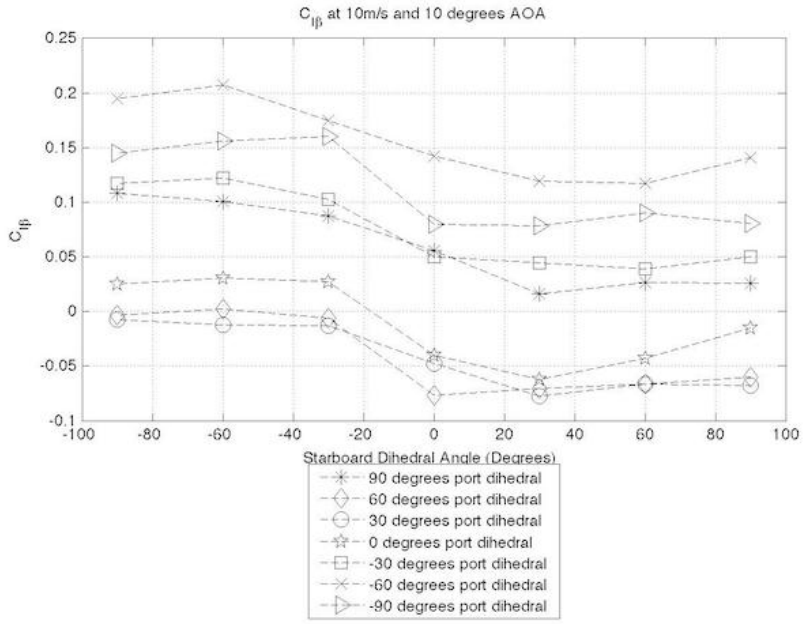

Figure 23: Lateral stability derivative variation

As Figure 23 shows, some configurations stabilise the aircraft in a sideslip condition whereas others de-stabilise it. A peak value of $C_{l\beta} = -0.077$ is generated at starboard dihedral of 60 degrees and 0 degree port dihedral. The aircraft selected for direct comparison is the Cessna 182 due to its similarity in planform and overall configuration. The rolling stability derivative

for this aircraft in a climb scenario is $C_{l\beta} = -0.0895$, a highly comparable value.

The rolling moment of an aircraft is produced by multiple sources, each with varying strength. In an ideal situation, the rolling moment produced would come solely from the main wing but certain data cases tell us this is not the case. Taking the configuration of 90 degrees port dihedral and 0 degrees starboard dihedral, the span-wise component of the force produced by the port wingtip would increase as the left sideslip angle increases, due to the increased AOA. The lift produced over the starboard wing should reduce with increased left sideslip angle due to a reduced chord-wise component of incoming flow. From just the wing contribution the stability derivative should be negative, indicating a stable aircraft. In fact, the stability derivative is positive when all factors are included. Due to the high wing configuration, the rolling moment due to the fuselage is acting to roll the aircraft further into the sideslip and its influence can be attributed to the counterintuitive data highlighted.

It is interesting to note that all positive-positive deflection angles in Figure 23 produce a laterally stable configuration, showing the effect of dihedral on the stability derivative. Similarly, the negative-negative deflection cases show a laterally unstable aircraft as a result of anhedral. This further validates the findings in the preceding section and shows that FOLDERONS can be used to modify the lateral stability if required to perform specific manoeuvres and demonstrate certain behaviour.

Directional Stability

Figures 24 and 25 present the same 10 degree AOA cases as presented for the lateral stability analysis. These figures represent the trend observed for all test cases. For an aircraft in a left hand sideslip, the yawing moment should be negative and in this case the base aircraft is directionally stable (designated by the horizontally dashed line). In a similar way to the lateral stability case, the wingtip configurations can act to both increase and decrease the stability. If both wingtips are symmetrically actuated to $\pm$ 90 degrees, the surfaces should create a force in the same direction as the vertical stabiliser and this in theory should produce a small moment due to the wingtip sweep angle. By observing the $\pm$ 90 degree symmetric actuation case in Figures 24 and 25, the restoring moment has improved over the planar wingtip case, though not by a significant amount; this is a good result and as predicted.

The largest increase in restoring moment is observed when the port wingtip is at a low positive dihedral angle and the starboard wingtip is at negative 90 degrees. In this scenario, the port wing is producing more lift than the starboard one and therefore the total drag value of the port wing is greatest. The increased drag differential creates a yawing moment in the direction of the sideslip velocity. Based on this, we can conclude that FOLDERONS can produce a restoring moment of varying magnitudes through two mechanisms and increase the directional stability of an already stable aircraft.

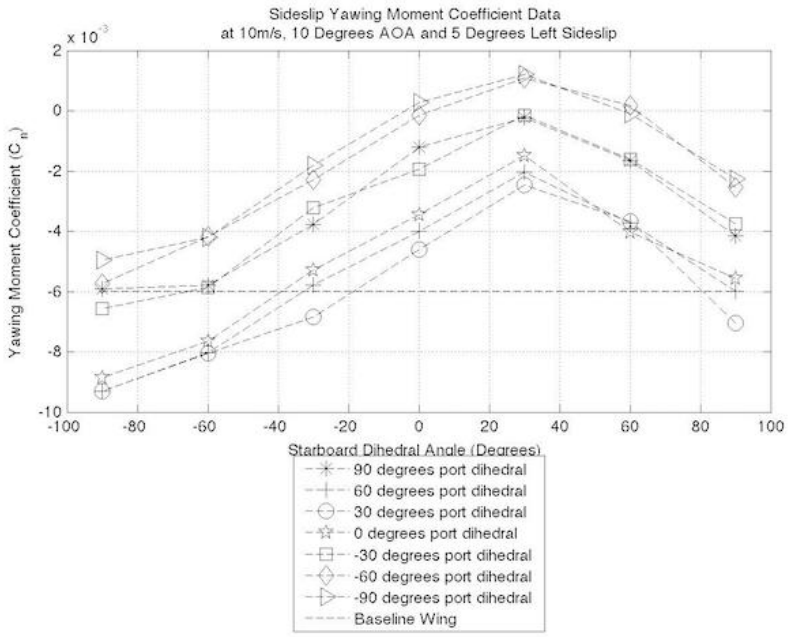

Figure 24: 5 degrees sideslip yawing moment coefficient

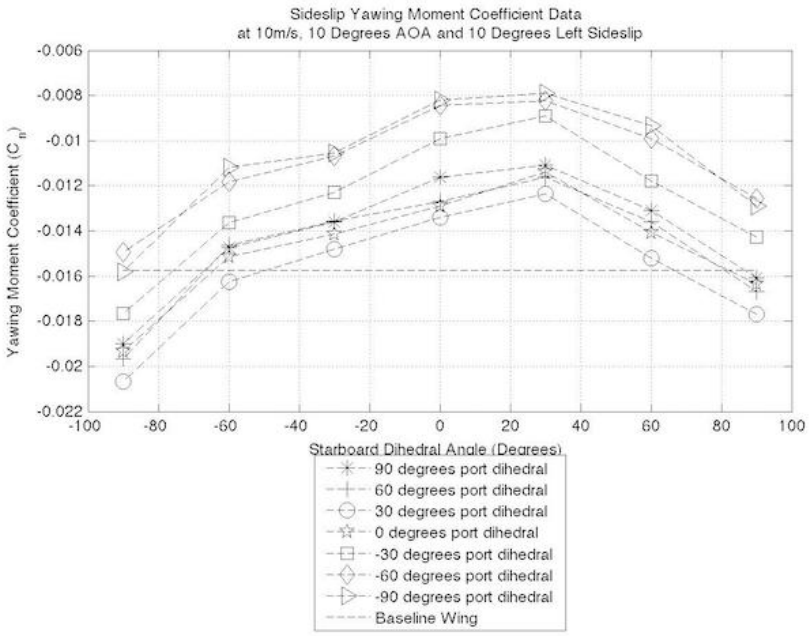

Figure 25: 10 degrees sideslip yawing moment coefficient

Real Aircraft Directional Stability Comparison

A plot of the directional stability derivative can be seen in Figure 26.

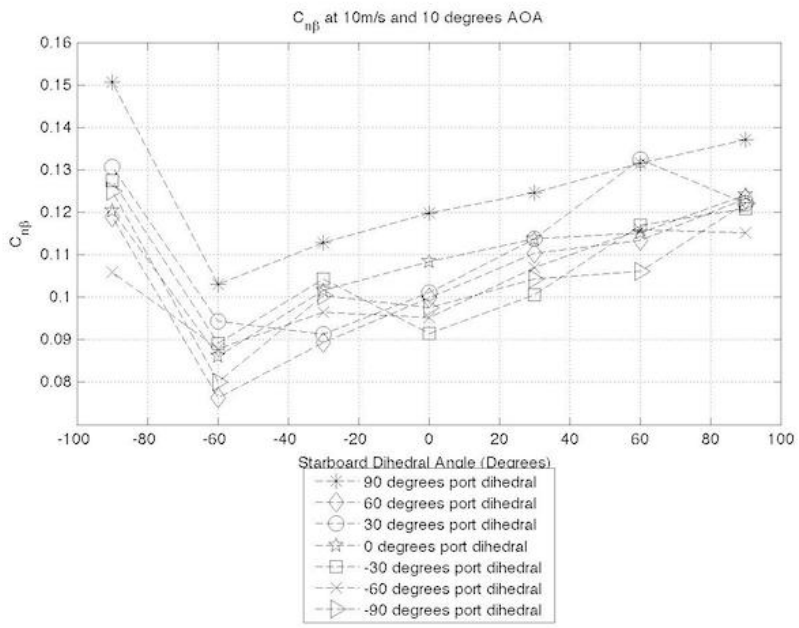

Figure 26: Directional stability derivative variation

For a stable aircraft in left hand sideslip, the directional stability derivative is positive. The figure shows that all configurations provide a positive derivative and therefore all configurations are directionally stable. The minimum positive value observed is $C_{n\beta} = 0.076$ which when compared to that of the Cessna 182 during climb, $C_{n\beta} = 0.0907$ shows that even the most de-stabilising configuration has a comparable value to that of a real aircraft. The maximum value of $C_{n\beta} = 0.151$ is significantly higher than that of the Cessna 182. The data collected shows that a 66% change in the directional stability derivative is available through the use of FOLDERONS. This is a property that could be harnessed for complex manoeuvre cases where a change in the directional stability is beneficial.

The maximum lateral stability derivative was observed at 60 degrees port dihedral and zero degrees starboard. The directional stability derivative for the same configuration is $C_{n\beta} = 0.100$, showing a positive correlation between lateral and directional stability derivatives.

VIII Conclusions

This report has shown that FOLDERONS can enhance the rolling authority of a conventional aircraft especially at high angles of attack or large dynamic pressure. These systems provide sufficient rolling authority (moment and rate) during the less demanding flight phases (mainly cruise. The rolling moment (direction and magnitude) generated by FOLDEDRONS is highly dependent on the angle of attack which is not the case for conventional ailerons. In fact, the mechanism of generating roll authority is very different between FOLDERONS and ailerons. Ailerons produce roll control by incremental lift on each side of the wing. On the other hand, FOLDERONS generate roll control by tilting the wingtip lift and reducing the moment arm on each side of the wing, hence the dependency on the AOA. Unlike ailerons, rolling authority generated using FOLDERONS suffers from reversal effect at negative angles of attack. In other words, at negative angles of attack, changing the dihedral angles of the wingtips to roll right produces a roll to the left instead. This destabilising contribution must be considered in the design of the control law and might pose issues if operated in steep descents/dives. The actuation speed of the FOLDERONS has a significant impact on their effectiveness. The maximum effectiveness of the FOLDERONS occurs when the actuation rates are in the same order of magnitude as the rate of the airflow to allow flow to develop around the wingtips as they fold. Due to the large deflection angles required from these systems, high actuation rates would be needed to meet response rate requirements, reducing the aerodynamic effectiveness. The lateral and directional stability are significantly affected by the FOLDERONS, allowing active tailoring of these values. For a conventional aircraft, stability is of paramount importance but too much stability can lead to an unresponsive and hard to manoeuvre aircraft. The ability to tailor these stability values leads to the notion of less resisted manoeuvre cases. Adjustment in these values allows an aircraft to be less resistive to control commands and ultimately lead to smaller control inputs and reduced control surface loading. In addition, cross coupling between the yaw and roll axes was observed. FOLDERONS have minimal impact on the pitch axis mainly due to the fact that the wing is straight. The addition of wing sweep would allow pitch axis authority and cross coupling between all 3 control axes to be achieved which might allow new types of manouvres to be acheived. It is suggested that further work is carried out to investigate the impact of, and the solution to, the gap covering problem. A compromise solution was used to good effect in this study but this is an area with improvement still to be made. The main issue with the current system is the lack of rolling moment developed at low speed and low AOA, a study should be carried out to investigate modifying the system to include wingtip twist to vary the wingtip AOA. If successful, this would increase the range of flight conditions the system can effectively operate in but must be traded off against the additional complexity introduced.

References

[1] M. A. Smith, ed., *Flight and Aircraft Engineer weekly*, vol. 65. Flight and Aircraft Engineer, January 1954.

[2] Advisory Council for Aviation Research and Innovation in Europe, "European aeronautics: A vision for 2020," January 2001.

[3] European Commission, "Flightpath 2050: Europe's vision for aviation," 2011.

[4] E. Kaygan and A. Gatto, "Investigation of adaptable winglets for improved uav control and performance," *World Academy of Science, Engineering and Technology*, vol. 8, no. 7, 2014.

[5] P. Bourdin, A. Gatto, and M. Friswell, "The application of variable cant angle winglets for morphing aircraft control," in *Applied Aerodynamic Conference*, 2006.

[6] D. Smith, M. Lowenberg, D. Jones, and M. Friswell, "Computatonal and experimental validation of the active morphing wing," *Journal of Aircraft*, vol. 51, June 2014.

[7] A. Gatto, P. Bourdin, and M. Friswell, "Experimental investigation into the control and load alleviation capabilities of articulated winglets," *International Journal of Aerospace Engineering*, vol. 2012, 2012.

[8] S. Barbarino, O. Bilgen, R. M. Ajaj, M. I, Friswell, and D. J.Inman, "A review of morphing aircraft," *Journal of Intelligent Material Systems and Structures*, vol. 22, 2011.

[9] D. P. Raymer, *Aircraft Design: A Conceptual Approach*, vol. 5. AIAA, 2012.

[10] "www.rcworld.com," September 2016.

[11] N. Ursache, T. Melin, A. Isikveren, and M. Friswell, "Technology integration for active poly-morphing winglets development," in *ASME Conference on Smart Materials*, 2008.

[12] C. R. Saff, "Airframe certification methods for unmanned aircraft," tech. rep., The Boeing Company, 2007.

[13] A. Slocum, "Fundamentals of design," tech. rep., MIT, 2008.

Nomenclature

Abbreviations

AOA Angle Of Attack

CAD Computer Aided Design

CFD Computational Fluid Dynamics

CNC Computer Numerical Control

$FOLDERONS$ FOLDing wingtips sERving as cONtrol effectorS

UAV Unmanned Aerial Vehicle

VLM Vortex Lattice Method

Symbols

α	Angle of Attack
$C_{\eta\beta}$	Directional Stability Derivative
C_{η}	Yawing Moment Coefficient
$C_{L\alpha}$	Lift Curve Slope
$C_{l\beta}$	Lateral Stability Derivative
C_{l}	Rolling Moment Coefficient
Λ	Wingtip Dihedral
Φ	Wingtip Twist
Ψ	Wingtip Sweep
ρ	Air Density
S_w	Wingtip Area
V	Velocity
b	Wingspan